nature genetics

Mutations in *LCA5*, encoding the ciliary protein lebercilin, cause Leber congenital amaurosis

Anneke I den Hollander[1,16], Robert K Koenekoop[2,16], Moin D Mohamed[3,4,16], Heleen H Arts[1,16], Karsten Boldt[5,6], Katherine V Towns[3], Tina Sedmak[7], Monika Beer[5,6], Kerstin Nagel-Wolfrum[7], Martin McKibbin[3,8], Sharola Dharmaraj[4], Irma Lopez[2], Lenka Ivings[3,9], Grange A Williams[3], Kelly Springell[3], C Geoff Woods[10], Hussain Jafri[11], Yasmin Rashid[12], Tim M Strom[5,6], Bert van der Zwaag[13], Ilse Gosens[1], Ferry F J Kersten[1], Erwin van Wijk[1], Joris A Veltman[1], Marijke N Zonneveld[1], Sylvia E C van Beersum[1], Irene H Maumenee[14], Uwe Wolfrum[7], Michael E Cheetham[15], Marius Ueffing[5], Frans P M Cremers[1,16], Chris F Inglehearn[3,16] & Ronald Roepman[1,16]

Leber congenital amaurosis (LCA) causes blindness or severe visual impairment at or within a few months of birth. Here we show, using homozygosity mapping, that the *LCA5* gene on chromosome 6q14, which encodes the previously unknown ciliary protein lebercilin, is associated with this disease. We detected homozygous nonsense and frameshift mutations in *LCA5* in five families affected with LCA. In a sixth family, the *LCA5* transcript was completely absent. *LCA5* is expressed widely throughout development, although the phenotype in affected individuals is limited to the eye. Lebercilin localizes to the connecting cilia of photoreceptors and to the microtubules, centrioles and primary cilia of cultured mammalian cells. Using tandem affinity purification, we identified 24 proteins that link lebercilin to centrosomal and ciliary functions. Members of this interactome represent candidate genes for LCA and other ciliopathies. Our findings emphasize the emerging role of disrupted ciliary processes in the molecular pathogenesis of LCA.

Leber congenital amaurosis is the most common cause of congenital blindness in infants and children. So far, mutations in eight genes and three chromosomal loci have been associated with autosomal recessive forms of LCA (OMIM 204000; RetNet). The LCA5 locus (OMIM 604537) on chromosome 6q was first identified in a consanguineous family (W06-873) of the Old Order River Brethren[1]. Linkage to the LCA5 locus has also been reported in a consanguineous family (MEP25) from Pakistan[2].

We performed genome-wide homozygosity mapping in nine additional consanguineous Pakistani LCA families, and in 33 consanguineous and 60 non-consanguineous affected individuals of various ethnic origins (that is, from various geographical regions). Two of the Pakistani families (MEP2 and MEP4), one consanguineous individual (patient 27240) from Morocco and one non-consanguineous individual (patient 28609) of Ashkenazi Jewish descent were homozygous for marker alleles at the *LCA5* locus (**Supplementary Tables 1** and **2** online). Families MEP2, MEP4 and MEP25 shared an identical homozygous 780-kb haplotype (**Supplementary Table 1**). Sequence analysis of the three genes in this interval identified a homozygous frameshift mutation (1151delC; P384QfsX17) in exon 6 of *C6ORF152* (now called *LCA5*) in all affected members of these three families (**Fig. 1a–c** and **Supplementary Fig. 1** online). Sequence analysis of *LCA5* identified a homozygous frameshift mutation (1476dupA; P493TfsX1) in exon 9 of patient 27240 and a homozygous nonsense mutation (835C>T; Q279X) in exon 5 of patient 28609 (**Fig. 1b,c** and **Supplementary Fig. 1**).

No mutation was detected in the coding exons or splice junctions of *LCA5* in the original LCA5 family W06-873. Further analysis of the *LCA5* gene, however, identified a homozygous deletion of 1598 bp (g.[−19612_−18015]del1598) in the affected individuals, encompassing 1,077 bp of the promoter region and noncoding

[1]Department of Human Genetics, Nijmegen Centre for Molecular Life Sciences, Radboud University Nijmegen Medical Centre, Nijmegen, The Netherlands. [2]McGill Ocular Genetics Center, McGill University Health Center, Montreal, Canada. [3]Section of Ophthalmology and Neurosciences, Leeds Institute of Molecular Medicine, St James's University Hospital, Leeds, UK. [4]Department of Ophthalmology, St Thomas' Hospital, London, UK. [5]Institute of Human Genetics, GSF National Research Center for Environment and Health, Munich-Neuherberg, Germany. [6]Institute of Human Genetics, Technical University Munich, Munich, Germany. [7]Institut für Zoologie, Johannes Gutenberg University, Mainz, Germany. [8]Eye Department, Chancellor Wing, St James's University Hospital, Leeds, UK. [9]Eye and Nutrition Research Group, FLAVIC, National Institute for Research on Agronomy, Dijon, France. [10]Department of Medical Genetics, Cambridge Institute for Medical Research, Addenbrooke's Hospital, Cambridge, UK. [11]Gene Tech Lab 146/1, Shadman Jail Road, Lahore, Pakistan. [12]Department of Obstetrics and Gynaecology, King Edward Medical University, Lahore, Pakistan. [13]Department of Pharmacology and Anatomy, Rudolf Magnus Institute of Neuroscience, University Medical Centre Utrecht, Utrecht, The Netherlands. [14]Wilmer Eye Institute, Johns Hopkins University, Baltimore, Maryland, USA. [15]Division of Molecular and Cellular Neuroscience, Institute of Ophthalmology, University College London, London, UK. [16]These authors contributed equally to this work. Correspondence should be addressed to A.I.d.H. (a.denhollander@antrg.umcn.nl).

Received 31 January; accepted 10 May; published online 3 June 2007; doi:10.1038/ng2066

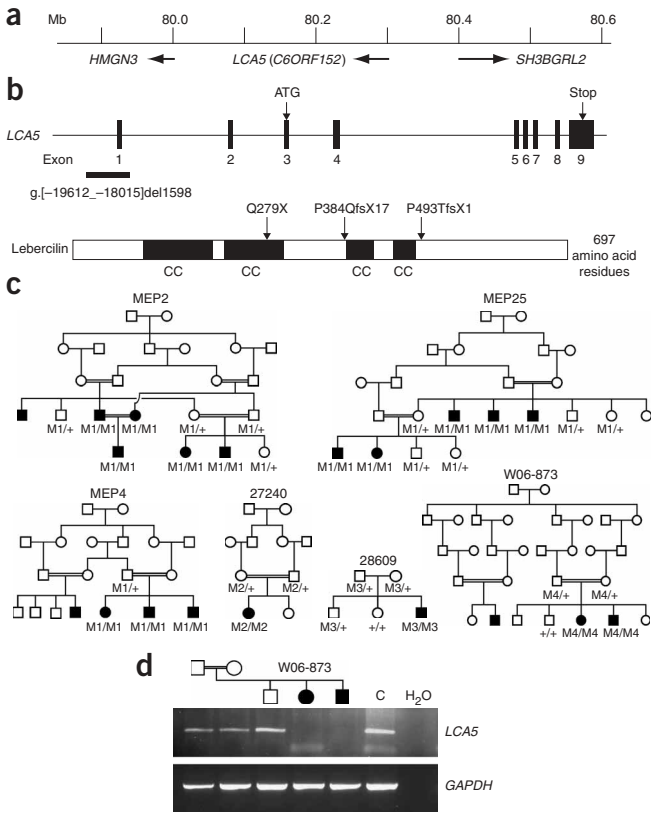

Figure 1 Molecular genetic analysis of the *LCA5* gene in families affected with LCA. (**a**) The LCA5 critical interval at 6q14, spanning 780 kb between 79.8 and 80.6 Mb from 6pter. Arrows indicate the location and transcription direction of three positional candidate genes. (**b**) Exon-intron structure of the *LCA5* gene and domain structure of the lebercilin protein. The start (ATG) and stop codons are indicated. Arrows indicate the locations of protein-truncating mutations; the bar indicates the location of the genomic deletion. CC, coiled coil region. (**c**) Pedigrees of LCA families showing homozygosity at the LCA5 locus. Four different mutations were identified in six LCA families: M1, 1151delC (P384QfsX17); M2, 1476dupA (P493TfsX1); M3, 835C>T (Q279X); M4, g.[−19612_−18015]del1598. (**d**) Expression analysis of the *LCA5* transcript in RNA isolated from fresh blood samples of family W06-873 by RT-PCR using a forward primer in exon 8 and a reverse primer in exon 9. The *LCA5* transcript was absent in the affected individuals. C, control individual. *GAPDH* was used as a positive control.

exon 1 (**Fig. 1b,c** and **Supplementary Fig. 1**). The *LCA5* transcript was absent in RNA isolated from fresh blood samples of the affected individuals of this family (**Fig. 1d**). None of the mutations was detected in more than 180 control individuals.

Patients 27240 and 28609, and the affected members of family W06-873 presented a severe congenital retinal dystrophy consistent with LCA (congenital visual loss, nystagmus, high hyperopia and a nondetectable electroretinogram), and had normal neurological and renal function[1]. The affected individuals of the three Pakistani families (MEP2, MEP4 and MEP25) were documented with poor vision from early infancy, and were otherwise healthy as far as could be established without detailed clinical testing[2].

Bioinformatic analysis of the 697–amino acid lebercilin protein identified four regions that are predicted to form coiled coils, but did not reveal other known functional motifs (**Fig. 1b**). Although a homology search indicated that this structure is weakly similar to several ciliary proteins, including CEP290, only one true homolog (C21ORF13) was identified. Lebercilin and C21ORF13 orthologs were identified in most mammalian genomes, whereas only one ortholog was found in lower taxa (**Supplementary Fig. 2** online). This observation suggests that lebercilin and C21ORF13 are derived from a common ancestor.

RT-PCR analysis showed that the *LCA5* gene is widely expressed in human tissues (**Supplementary Fig. 3a** online). Expression analysis of the gene throughout mouse development by mRNA *in situ* hybridization revealed an almost ubiquitous, low-level staining at 12.5 days post coitum (d.p.c.; **Fig. 2a**). At later stages (embryonic day 14.5 (E14.5), E16.5 and E18.5), staining of the eye, inner ear, kidney, regions of the central and peripheral neural system, the gut and the ciliated epithelium of the nasopharynx, trachea and lungs was more pronounced (**Fig. 2b–g**). This expression is consistent with the reported presence of lebercilin in the proteome of ciliary axonemes of human bronchial epithelial cells[3,4]. Expression in the mouse eye shifted during development from the ganglion cell layer to the photoreceptors (**Fig. 2h–k**). In adult eyes (postnatal day 90; P90), expression was limited to the photoreceptor cell layer (**Fig. 2k**).

A polyclonal antibody directed against lebercilin (anti-lebercilin) detected a 100-kDa signal in human retinal homogenates (**Fig. 3a**) and

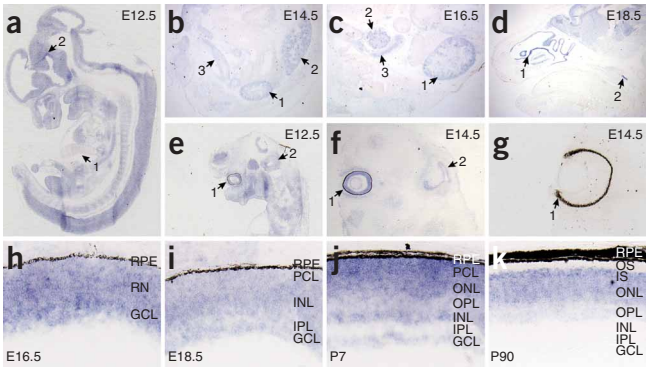

Figure 2 Analysis of *Lca5* expression in mouse embryos and adult eyes by mRNA *in situ* hybridization. (**a**) At E12.5, the gene appeared to be ubiquitously expressed in all tissues apart from the liver (1). In the brain, the zona limitans intrathalamica (2) showed more staining than surrounding structures. (**b**) At E14.5, staining was more pronounced in the kidneys (1), lung (2) and the gut (3), suggestive of higher *Lca5* expression. (**c**) At E16.5, prominent staining was detected in the kidney (1), testis (2) and mesonephric tissue (3). (**d**) At E18.5, intense staining was noted in the nasopharynx (1), trachea and Eustachian tube (2). (**e**,**f**) Expression in the developing eye (1), including neural retina and lens, and in the developing inner ear (2) was observed at E12.5 (**e**) and was more pronounced at E14.5 (**f**). (**g**) A sense cRNA probe revealed no staining in the eye (or other tissues; not shown), indicating the specificity of the assay (1, pigment of the RPE). (**h–k**) Magnification of the retinal cell layers. (**h**) At E16.5, staining was slightly more pronounced in the layer that differentiates into the ganglion cells. (**i**) At E18.5, expression appeared to be slightly higher in the neural layer than in the ganglion cell layer and the photoreceptor cells. (**j**) In juvenile eyes, expression was detected in all retinal cells. (**k**) In adult eyes, expression was limited to the photoreceptor layer. RPE, retinal pigment epithelium; RN, retinal neurons; GCL, ganglion cell layer; PCL, photoreceptor cell layer; INL, inner nuclear layer; IPL, inner plexiform layer; ONL, outer nuclear layer; OPL, outer plexiform layer; OS, outer segments; IS, inner segments.

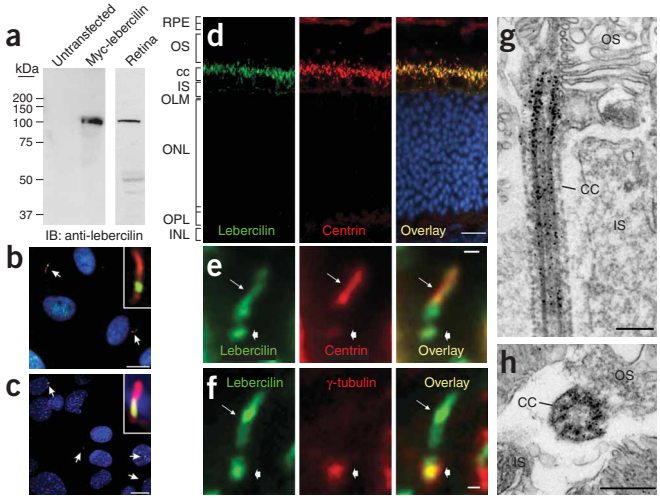

Figure 3 Localization of lebercilin to cilia of cultured cells and mouse photoreceptor connecting cilia. (**a**) Immunoblot (IB) analysis of the specificity of anti-lebercilin. A 100-kDa signal was detected in human retinal homogenates (right) and SK-N-SH cells transfected with recombinant Myc-lebercilin (middle). No signal was observed in the untransfected cell lysates (left). (**b**,**c**) Staining of endogenous lebercilin in ARPE-19 (**b**) and IMCD3 (**c**) cells using anti-lebercilin (green) and anti-acetylated tubulin as an axonemal marker (red). Lebercilin was detected at the base of the primary cilia (arrows, and magnified in insets). (**d**) Subcellular localization of lebercilin in radial cryosections of mature mouse retina using anti-lebercilin (green) and anti-pan-centrin (red), a marker for the photoreceptor ciliary apparatus[5]. The overlay shows the colocalization of lebercilin with centrins (yellow) in the region of connecting cilia of photoreceptors. (**e**,**f**) High magnification of single photoreceptor cilia double labeled with anti-lebercilin (green) and anti–pan-centrin (red; **e**), and anti-γ-tubulin (red; **f**) as markers for the connecting cilium (thin arrows) and/or the centrioles of the basal bodies (thick arrows), respectively. Overlays showed colocalization of lebercilin with centrins in the connecting cilium (thin arrows) and in the basal bodies, where lebercilin also colocalized with γ-tubulin (thick arrows). (**g**,**h**) Immunoelectron microscopy of part of a mouse rod photoreceptor cell labeled with anti-lebercilin. Analysis of longitudinal (**g**) and transversal (**h**) ultrathin section through the connecting cilium showed lebercilin localization at the ciliary microtubules with a concentration at the apical part of the connecting cilium. Scale bars, 10 μm (**b**–**d**); 0.3 μm (**e**, **f**); 0.2 μm (**g**,**h**). Nuclei were stained with DAPI (blue; **b**–**d**). CC, connecting cilia; OLM, outer limiting membrane.

in several mouse tissues (**Supplementary Fig. 3b**). In ciliated cells (ARPE-19 and IMCD3), staining with anti-lebercilin showed that the endogenous protein localizes to the ciliary axoneme, with increased amounts at the base of the primary cilia (**Fig. 3b**,**c**). Immunohistochemical analysis of mouse and rat retinae revealed a clear punctate pattern of localization in a narrow region between the outer and inner segments of the photoreceptor layer (**Fig. 3d**). Costaining with monoclonal antibodies to centrins (Cen1–Cen4; ref. 5) and γ-tubulin as markers for connecting cilia and basal bodies, respectively, showed that lebercilin is localized in the connecting cilium and the basal bodies of photoreceptor cells (**Fig. 3e**,**f**). High-resolution analysis by immunoelectron microscopy confirmed the ultrastructural localization of lebercilin to the axonemal microtubules of the connecting cilium (**Fig. 3g**,**h**). This ciliary localization of lebercilin in the retina suggests that LCA5 is a ciliopathy.

Localization to the cilia was also observed in ARPE-19 cells expressing recombinant lebercilin fused with enhanced yellow fluorescent protein at its C terminus (lebercilin-eYFP; **Fig. 4**). Most prominent staining was often observed at the basal body and transition zone of the cilium (**Fig. 4d** and **Supplementary Fig. 4** online). In cells expressing larger amounts of lebercilin-eYFP, the protein was prominently associated with both cilia and microtubules (**Fig. 4b**). Numerous cells also showed a perturbed microtubule cytoskeleton with long and wavy microtubule bundles stained with fluorescent lebercilin (**Fig. 4c** and **Supplementary Fig. 4**). Similar observations have been made on overexpression of fragments of the centrosomal protein CEP170 (a mature centriole marker[6]) and the dynactin subunit $p150^{glued}$ (ref. 7), and on inhibition of the motor protein cytoplasmic dynein[8], which suggests that overexpression of lebercilin disturbs microtubule dynamics. In COS-1 cells containing a centrosome, lebercilin-eYFP was associated with the microtubules radiating from this microtubule-organizing center (**Fig. 4e**). Depolymerization

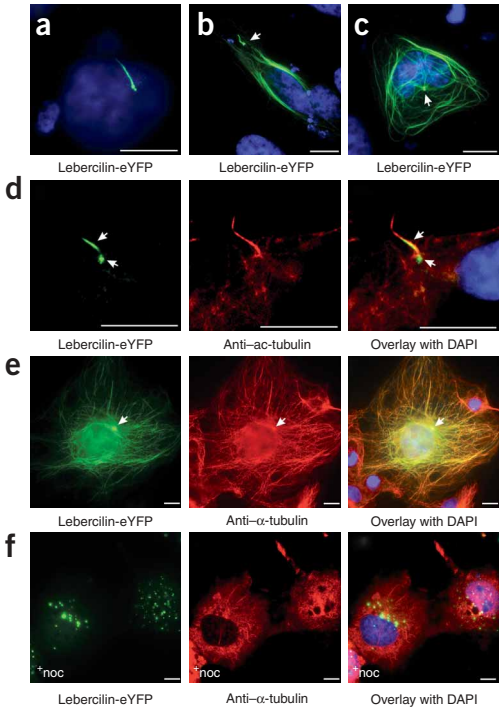

Figure 4 Subcellular localization of recombinant lebercilin-eYFP in cultured mammalian cells. (**a**–**d**) ARPE-19 cells. (**e**,**f**) COS-1 cells. Nuclei were stained by DAPI (blue). (**a**) Localization of lebercilin-eYFP (green) at the axoneme and basal body of the primary cilium. (**b**) Higher expression of lebercilin showed microtubule localization in addition to ciliary (arrow) localization. (**c**) Long, thick and wavy microtubules, indicating microtubule bundling, were stained with lebercilin-eYFP. Arrow indicates the centrosome. (**d**) Magnification of the cilium revealed an enhanced green signal at the basal body and the transition zone, and a decrease in signal intensity towards the tip of the cilium (left), which was visualized with anti–acetylated tubulin (center, red). Right, overlay of lebercilin-eYFP and anti–acetylated tubulin. (**e**) In nonciliated COS-1 cells, lebercilin colocalized with the centrosome (arrow) and its associated cellular microtubule array (left). Costaining with anti–α-tubulin (center) confirmed colocalization of lebercilin with microtubules (right, yellow). (**f**) Depolymerization of the microtubules by nocodazole treatment abrogated the microtubule association of lebercilin, as indicated by the dispersed punctate green signal. Scale bars, 10 μm.

Table 1 TAP and LC-MSMS analysis of the lebercilin interactome in HEK293 cells

			Identified in *x* of 2 analyses[a]	
Swissprot ID	Human protein	Description	Lebercilin-NTAPe	Lebercilin-CTAPe
Q86VQ0	CF152	Lebercilin	2	2
Adaptor proteins				
P62258	1433E	14-3-3ε	2	2
P31946	1433B	14-3-3β/α	2	2
P61981	1433G	14-3-3γ	2	2
P63104	1433Z	14-3-3ζ/δ	2	2
P27348	1433T	14-3-3θ	2	2
Q04917	1433F	14-3-3η	1	1
Cytoskeletal and associated proteins				
P06748	NPM	Nucleophosmin	1	1
P19338	NUCL	Nucleolin	2	2
P63167	DYL1	Dynein light chain 1	1	1
Q96FJ2	DYL2	Dynein light chain 2, cytoplasmic	1	
Cellular signaling proteins				
P67870	CSK2B	Casein kinase II subunit β	2	2
P68400	CSK21	Casein kinase II subunit α	2	2
P19784	CSK22	Casein kinase II subunit α′	2	1
Q01105	SET	Phosphatase 2A inhibitor I2PP2A	2	
Chaperones and co-chaperones				
P08107	HSP71	Heat shock 70-kDa protein 1	2	2
P11142	HSP7C	Heat shock cognate 71-kDa protein	2	2
P11021	GRP78	78-kDa glucose-related protein	2	2
P34931	HS70L	Heat shock 70-kDa protein 1L	1	
P38646	GRP75	Stress-70 protein	2	2
Miscellaneous				
Q96S59	RANB9	Ran-binding protein 9	2	1
P55209	NP1L1	Nucleosome assembly protein 1-like 1	2	
Q14241	ELOA1	Transcription elongation factor B polypeptide 3	2	
Q93008	USP9X	Ubiquitin thioesterase FAF-X	1	
Q07021	C1QBP	Glycoprotein gC1qBP	1	1

[a]Lebercilin tagged at the N or C terminus was purified by TAP. Eluates were precipitated and subjected to tryptic digestion before direct analysis by LC-MS/MS. Protein and peptide summaries of these analyses are given in **Supplementary Table 3**.

of the microtubules by nocodazole treatment abrogated the microtubular localization (**Fig. 4f**). Recombinant lebercilin fused with a fluorescent monomeric red fluorescent protein (mRFP) protein at its N terminus showed a similar ciliary and microtubule-governed localization (**Supplementary Fig. 4**). Colocalization of lebercilin with the centriole marker γ-tubulin at the mother centriole of the centrosome (**Supplementary Fig. 4**) matched the localization to its counterpart in cilia, the basal body.

We next generated fusion proteins of lebercilin that were tagged at the N or C terminus to identify proteins that interact with lebercilin. To enforce a bias for true positive interactions, we applied tandem affinity purification (TAP)[9] of the protein complexes in their native functional states from human embryonic kidney 293 (HEK293) cells, and analyzed the purified complexes by liquid chromatography coupled with tandem mass spectrometry (LC-MS/MS; **Table 1**, and **Supplementary Table 3** online). In these cells, recombinant lebercilin also localized to the microtubules and centrosomes (data not shown).

The interactome identified consists of 24 proteins, many of which have previously been associated with microtubules and/or have important centrosomal or ciliary functions. An important association was found with cytoplasmic dynein, strengthening the link between lebercilin and microtubule dynamics and suggesting that lebercilin might be involved in minus end–directed microtubule transport. Another interactor, nucleophosmin, is known to localize to centrosomes[10], where it is involved in the regulation of centrosome duplication by interaction with ROCKII (ref. 11); it also functions as a substrate of Polo-like kinase 1, a key regulator of centrosome function[12], and has been found to bind to RPGR, a protein involved in X-linked retinal dystrophies[13]. Like nucleophosmin, the interacting protein nucleolin is a mainly nuclear multifunctional protein involved in nucleocytoplasmic shuttling[14], and binds to casein kinase 2 (CK2) in photoreceptors[15,16]. CK2 is also present in the lebercilin interactome and has been found to regulate microtubule dynamics[17], to localize to the centrosome[18] and to modulate the localization of several proteins to cilia through phosphorylation[19,20]. Lastly, lebercilin interacts with 14-3-3 scaffold proteins, which bind and regulate the function of many phosphorylated proteins[21] and associate with centrosomal protein complexes[22,23]. Taken together, these interactions and its subcellular localization implicate lebercilin as a ciliary and microtubule-associated protein.

To confirm that the identified lebercilin interactome is present in the retina, we used anti-lebercilin to immunoprecipitate quantitatively

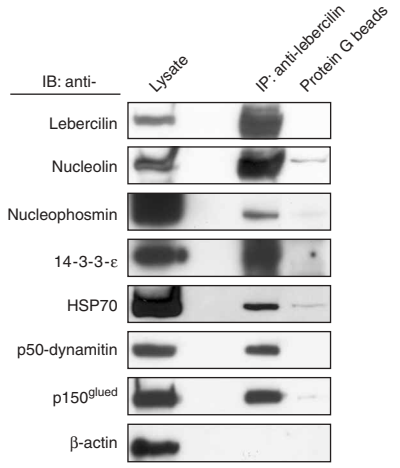

Figure 5 Analysis of the lebercilin interactome in porcine retina. Lebercilin was immunoprecipitated with anti-lebercilin from 500 μg of porcine retinal lysate. The purified protein complex was separated by SDS-PAGE and immunoblotted with antibodies specific to proteins identified by LC-MS/MS after TAPe complex purification. Nucleolin, nucleophosmin, 14-3-3ε, HSP70, and the dynactin subunits p50-dynamitin and p150^{glued} bound specifically to lebercilin. β-actin was used as a negative control for the specificity of the immunoprecipitation.

the lebercilin-associated protein complex from porcine retinal extracts (**Supplementary Fig. 5** online). Using antibodies specific to a few members of the identified interactome on immunoblots of the anti-lebercilin immunoprecipitate, we correlated our TAP findings *in vivo* (**Fig. 5**). Nucleophosmin, nucleolin, 14-3-3ε and HSP70, in addition to the dynein-binding dynactin subunits p50-dynamitin and p150^{glued}, were found to coimmunoprecipitate with lebercilin from retinal extracts. This finding strengthens the relevance of the interactome that we describe here with respect to the retinal disease mechanism of LCA.

Ciliary and centrosomal proteins are renowned for their involvement in various ciliopathies, including Bardet-Biedl syndrome, Joubert syndrome, Senior-Løken syndrome, Meckel-Gruber syndrome and nephronophthisis. LCA and Joubert syndrome have been recognized as allelic disorders that can be caused by mutations in the centrosomal and ciliary protein CEP290, providing evidence that some forms of LCA belong to this heterogeneous group of ciliopathies[24–27]. With the exception of *CEP290*, all previously identified LCA-associated genes are expressed preferentially in the eye, and have highlighted various defective processes in LCA, including phototransduction (*GUCY2D*), vitamin A metabolism (*RPE65*, *RDH12*), photoreceptor development (*CRX*), cell polarity (*CRB1*), protein biosynthesis (*AIPL1*), and intracellular protein transport (*RPGRIP1*). Identification of *LCA5* mutations in the ciliary protein lebercilin emphasizes the emerging role of disrupted ciliary processes in the pathogenesis of LCA. In addition to RPGRIP1, CEP290 and lebercilin, two proteins involved in retinitis pigmentosa, RPGR and RP1, have been shown to localize to the connecting cilia of photoreceptor cells.

On the one hand, the broad expression pattern of lebercilin throughout development, with pronounced expression in the kidney and the brain in late embryonic stages, suggests that this protein might also be involved in other ciliopathies such as Joubert syndrome. On the other hand, the observation that null mutations cause a phenotype only in the eye may instead point to functional redundancy in other tissues. Our study suggests that the genes encoding the lebercilin interactome should also be considered as candidate genes for LCA and other ciliopathies.

METHODS

Human samples. We obtained blood samples and pedigrees after receiving informed consent from all individuals. Approval was obtained from the Institutional Review Boards of the participating centers. Genomic DNA was isolated from lymphocytes by standard procedures. RNA was isolated from fresh blood samples with a PAXgene Blood RNA kit (Qiagen).

Homozygosity mapping, mutation analysis and RT-PCR. Genome-wide linkage scans in nine Pakistani families (64 individuals) were performed by using microsatellite genotypes generated by the Marshfield Free Genotyping Service screening set 11 (C.F.I. *et al.*, unpublished data). High-resolution haplotype analysis at the LCA5 locus was done with known microsatellite markers, short tandem repeats and SNPs selected from the UCSC Genome Browser. Microsatellites were genotyped on an ABI 3130 automated sequencer and analyzed with ABI Genotyper software, whereas SNPs were analyzed by direct sequencing. We carried out homozygosity mapping in 33 consanguineous and 60 non-consanguineous individuals with LCA from various ethnic origins with 10K, 100K or 250K Affymetrix SNP arrays (A.I.d.H. *et al.*, unpublished data).

Primers for PCR and sequencing of the nine exons and splice junctions of *LCA5* are given in **Supplementary Table 4** online. The expression of *LCA5* in blood samples, human tissues and mammalian cell lines was analyzed by RT-PCR on total RNA samples using a forward primer in exon 8 and a reverse primer in exon 9.

DNA constructs. We generated *LCA5* constructs by PCR using IMAGE clones of full-length human (BC050327) or mouse (BC052060) cDNA as a template. IMAGE clones were obtained from the Deutsches Ressourcenzentrum fuer Genomforschung (RZPD). Gateway-adapted constructs were created by using the Gateway cloning system (Invitrogen) according to the manufacturer's procedures.

Bioinformatic analysis. We searched protein and translated nucleic acid sequence databases for homologs using the BLAST programs. Protein sequences were searched for conserved functional patterns by using the InterProScan search tool of the protein signature databases PROSITE, PRINTS, ProDom, Pfam, SMART, TIGRFAMs, PIRSF, SUPERFAMILY, Gene3D and PANTHER. A similarity plot was generated with the Vector NTI software package (Invitrogen). A phylogenetic tree was created with TreeFam.

RNA *in situ* hybridization. Two 1-kb fragments of *Lca5*, located at the 3′ end of the gene, were selected to generate specific probes for RNA *in situ* hybridization. Sequences of the primers used to amplify these fragments are given in **Supplementary Table 4**. *Mus musculus* RIKEN cDNA 4930431B11 was used as a template. The PCR products obtained were cloned in the pCR4-TOPO vector (Invitrogen), verified by sequencing, and subsequently amplified by PCR using T7- and T3-polymerase specific oligonucleotide primers. Digoxigenin (DIG)-cRNA probes were generated as described[28], compared with a control DIG-cRNA probe (Roche), and stored at −80 °C.

Mouse embryos were collected at various embryonic stages (12.5 d.p.c. to 18.5 d.p.c.), and mouse eyes were collected at two postnatal stages (7 d and 90 d), frozen on crushed dry ice, and stored at –80 °C. We embedded the embryos and eyes in Tissue-Tek OCT compound (Sakura Finetek) and cut them into 16-μm sagittal sections at −16 to −20 °C. Sections were collected on SuperFrost Plus microscope slides (Menzel-Gläser), quickly dried and stored at −80 °C until further use. The DIG-labeled cRNA probes were then hybridized to the mouse tissue sections as described[28]. Slides were dehydrated by an alcohol series (30, 50, 70, 96 and 100% ethanol for 1 min each, followed by xylol twice for 3 min), and sealed with Entellan rapid mounting media (ProSciTech). Images were recorded on an Axioskop2 Plus microscope (Zeiss) with a power HAD DXC-950P 3CCD color video camera (Sony), and processed with Adobe Photoshop CS2 (Adobe Systems).

Generation of anti-lebercilin. Rabbit polyclonal antisera to lebercilin were raised against two peptides derived from the predicted amino acid sequence by

Eurogentec. The peptides (N-terminal residues 2–16, GERAGSPGTDQERKA; and C-terminal residues 661–674, EGRSFNPNRHRLKH) were conjugated to hemocyanin through a C-terminal (2–16) or N-terminal (660–674) cysteine residue before immunization. Final bleeds from two immunized rabbits were affinity-purified against both peptides by Eurogentec (Double XP program), and the affinity-purified sera were used in all subsequent experiments.

Protein blotting. Several tissues from male C57BL/6 mice, age 5 weeks, were freshly lysed and homogenized in SDS-PAGE sample buffer (at 0.1 g/ml), heated to 95 °C for 3 min, sonicated, and clarified by centrifugation (15,000*g*). Samples containing 100 µg of total protein from each tissue were immediately resolved by SDS-PAGE and analyzed by standard protein blotting techniques. We used anti-lebercilin at a 1:500 dilution. Untransfected SK-N-SH cells and cells transfected with a Myc-lebercilin expression construct using Lipofectamine Plus (Invitrogen) were used as a positive control.

Cell culture, transfection and fluorescence microscopy. All cells were grown at 37 °C in DMEM (Gibco), supplemented with 10% FCS, 100 IU/ml of penicillin, 1% Glutamax (Gibco) and 100 µg/ml of streptomycin. Fluorescent protein variants fused to full-length lebercilin were expressed in COS-1 and ARPE-19 cells by using pDest-733 (N-terminal mRFP tag) and pDest-504 (C-terminal eYFP tag) as described[29] with minor variations. Cells were seeded on glass slides (0.2×10^6 cells per slide) and grown for 48 h to 85–90% confluence. The cells were then transfected by using Effectene (Qiagen) according to the manufacturer's procedures, grown for 24 h, fixed with 4% paraformaldehyde, mounted in Vectashield mounting medium, with or without 4′,6′-diamidino-2-phenylindole (DAPI; Vector Laboratories), and analyzed by fluorescence microscopy as described[29]. We confirmed expression of the recombinant protein constructs by protein blotting (**Supplementary Fig. 4b**).

Immunocytochemistry. COS-1, ARPE-19 and IMCD3 cells were grown on glass slide coverslips and fixed either with 4% paraformaldehyde for 20 min or with methanol at −20 °C for 10 min. After fixation in 4% paraformaldehyde, the slides were washed twice in 50 mM glycine in PBS for 5 min, and then incubated in 1% Triton X-100 in PBS for 5 min. The washing steps in 50 mM glycine in PBS were then repeated. The slides were incubated with primary antibody for 1 h in 50 mM glycine and 5% FCS in PBS, blocked twice with 50 mM glycine and 5% FCS in PBS for 10 min, and then incubated with secondary antibody for 30 min. After removal of the unbound secondary antibody by three wash steps of 50 mM glycine in PBS, the slides were mounted in Vectashield mounting medium with or without DAPI (Vector Laboratories or Calbiochem). After fixation in methanol, the slides were washed twice in PBS and blocked with 2% BSA in PBS for 20 min. The subsequent steps were identical to those used for the paraformaldehyde-fixed slides.

The primary antibodies were affinity-purified rabbit anti-lebercilin (1:200 dilution), rat anti–α-tubulin (1:500 dilution, Serotec), mouse monoclonal anti–acetylated α-tubulin (1:250 dilution, Zymed Laboratories; or 1:1,000 dilution, Sigma), mouse monoclonal anti–γ-tubulin (1:1,000, affinity-purified, clone GTU-88, Sigma). The secondary antibodies were Texas red–conjugated goat anti-rabbit IgG (1:300, Molecular Probes), Alexa Fluor 568–conjugated goat anti-mouse (1:300, Molecular Probes), goat anti-rabbit 488 FITC (1:300, Molecular Probes), and chicken anti-mouse 594 TRITC (1:300, Molecular Probes). For microtubule depolymerization, transfected cells were incubated with 20 µM nocodazole for 2 h before fixation. Fluorescence was visualized with an Axioskop2 Mot Plus fluorescence microscope (Zeiss) equipped with a 63× oil immersion objective, or with an Eclipse TE2000-E microscope (Nikon) at 100× magnification. Photographs were taken with an AxioCam MRC5 camera (Zeiss).

Immunohistochemistry of retinal tissue. Eyes from a Wistar rat age 20 d and from C57BL/6J mice were isolated and physically fixed in melting isopentane at −168 °C (ref. 5). Cryosections (10 µm) were treated with 0.01% Tween-20 in PBS, and then blocked with blocking solution (0.1% ovalbumin and 0.5% fish gelatin in PBS). Antibodies against pan-centrin (centrin isoforms Cen1–Cen4, ref. 5; 1:2 of hybridoma supernatant), γ-tubulin (clone GTU-88, Sigma) and lebercilin diluted in blocking solution were incubated overnight at 4 °C. Secondary antibodies, Alexa Fluor 568–conjugated goat anti-mouse and Alexa Fluor 488–conjugated goat anti-rabbit (1:400, Molecular Probes) were also diluted in blocking solution and incubated for 1 h. Sections were embedded in Mowiol 4.88 (Hoechst). Fluorescence was analyzed with a DMRP microscope (Leica) equipped with an ORCA ER charge-coupled device camera (Hamamatsu). Images were processed with Adobe Photoshop CS2.

Pre-embedding immunoelectron microscopy. We carried out labeling as described[30]. Vibratome sections through mouse retinas were stained by anti-lebercilin and visualized by appropriate secondary antibodies (Vectastain ABC kit, Vector Laboratories). After fixation in 0.5% OsO_4, specimens were embedded in araldite and ultrathin sections were analyzed with a FEI Tecnai 12 Biotwin transmission electron microscope.

TAP. HEK293 cells transiently expressing the TAPe-tagged constructs were lysed in lysis buffer containing 50 mM Tris-HCl (pH 7.4), 150 mM NaCl, 0.5% Nonidet-P40, protease inhibitor cocktail (Roche) and phosphatase inhibitor cocktail 2 (Sigma-Aldrich) for 20 min at 4 °C. After sedimentation of nuclei at 10,000*g*, the cleared supernatant was incubated for 2 h at 4 °C with Strep-Tactin superflow (IBA). Subsequently, the resin was washed three times in wash buffer containing 50 mM Tris-HCl (pH 7.4), 150 mM NaCl, 0.1% Nonidet-P40 and phosphatase inhibitors. Protein baits were eluted with desthiobiotin (2 mM in TBS). For the second purification step, the eluates were transferred to anti-Flag M2 agarose (Sigma) and incubated for 2 h at 4 °C. The beads were washed three times with wash buffer and proteins were eluted with Flag peptide (200 µg/ml, Sigma-Aldrich) in TBS. After purification, the samples were either separated by SDS-PAGE and stained with silver according to standard protocols, or precipitated with chloroform and methanol.

Mass spectrometry. For LC-MS/MS analysis, samples were redissolved in 1 mM Tris (pH 8) and treated with 0.1 mg/ml of trypsin (sequencing-grade, Promega) overnight at 37 °C. After tryptic proteolysis, trifluoroacetic acid (TFA) was added to a final concentration of 0.5%. We carried out peptide separation by HPLC on an UltiMate nano-LC system (Dionex) equipped with a 75-µm C18 column. The mobile phases were 5% acetonitrile and 0.1% TFA (solution A), and 80% acetonitrile and 0.1% TFA (solution B). Peptides were separated by a gradient of 5–50% solution B over 140 min, followed by a gradient of 50–100% solution B over 5 min at a flow rate of 200 nl min^{-1}. The eluate was collected in 20-s fractions, which were spotted on matrix-assisted laser desorption ionization (MALDI) targets, diluted fourfold in 2.5 mg/ml of α-cyano-4-hydroxycinnamic acid (CCA), 70% acetonitrile and 0.1% TFA, by a Probot liquid handling system (Dionex). MS/MS analysis was performed on a MALDI time-of-flight tandem mass spectrometer (ABI 4700 Proteomics Analyzer, Applied Biosystems). MS/MS queries were done with the MASCOT search engine (Matrix Science) embedded in the GPS Explorer software (Applied Biosystems) against the Swiss Prot database. Proteins were considered to be identified when they were represented by at least two unique peptides with a MASCOT ion score >35 (confidence interval (C.I.) > 99%), or at least one peptide with a MASCOT ion score >70 (C.I. > 99.999%).

Coimmunoprecipitation from retinal protein lysates. Fresh porcine retinae were immediately stabilized with protease inhibitors (Roche), homogenized and solubilized for 30 min on ice with 1% *n*-dodecyl β-D-maltoside (Sigma) in immunoprecipitation buffer containing 150 mM NaCl, 1 mM EDTA, 20 mM Tris (pH 7.4) and protease inhibitor cocktail (Roche). Insoluble material was removed by centrifugation (57,000*g*) for 1 h at 4 °C. We adjusted 500 µg of retinal lysate with immunoprecipitation buffer to a protein concentration of 1 µg/µl and pre-cleared it for 30 min at 4 °C with Protein G Plus-Agarose (Santa Cruz Biotechnology). The pre-cleared lysate was mixed with anti-lebercilin (1,6 µg per 100 µg of total protein) and incubated at 4 °C overnight. Protein G Plus-Agarose was subsequently added for 1 h. Proteins were eluted with Laemmli buffer (containing 500 mM β-mercaptoethanol) for 15 min at room temperature (20 °C). Samples were resolved by SDS-PAGE and analyzed by standard protein blotting techniques. We used the following primary antibodies: rabbit polyclonal anti-nucleolin (Sigma), mouse monoclonal anti-nucleophosmin (Sigma; clone FC82291), rabbit polyclonal anti-14-3-3ε (Santa Cruz Biotechnology), mouse monoclonal anti-HSP70 (Sigma, clone BRM-22), monoclonal mouse anti–p50-dynamitin (Beckton Dickinson, clone 25), monoclonal mouse anti-$p150^{glued}$ (Beckton Dickinson), anti–β-actin (Sigma, clone AC-15). The secondary antibodies were goat anti-mouse–HRP and goat anti-rabbit (both Dianova).

URLs. Online Mendelian Inheritance in Man (OMIM), http://www.ncbi.nlm.nih.gov/entrez/query.fcgi?db=OMIM; RetNet, http://www.sph.uth.tmc.edu/Retnet/; Marshfield Free Genotyping Service screening set, http://research.marshfieldclinic.org/genetics/GeneticResearch/sets/Set11Info.xls; UCSC Genome Browser, http://genome.ucsc.edu/; InterProScan, http://www.ebi.ac.uk/InterProScan/; BLAST and PSI-BLAST, http://www.ncbi.nlm.nih.gov/BLAST/; Treefam, http://www.treefam.org.

Accession numbers. GenBank: human *LCA5* (*C6ORF152*) cDNA, NM_181714; human *C21ORF13* cDNA, NM_152505.

Note: Supplementary information is available on the Nature Genetics website.

ACKNOWLEDGMENTS

We thank the LCA families for their participation; H. Brunner, C. Johnson, N. Knoers and H. Kremer for discussions; C.J. Gloeckner for the TAPe constructs; T. Goldmann, E. Sehn, J. Hehir-Kwa, I. Janssen, K. Voesenek, A. Schumacher and S. Schöffmann for technical assistance; K. Klima, R. Pigeon and C. Robert for organizing the clinical data from affected individuals; S. Yzer, L.I. van den Born, S. Kohl, B. Wissinger, E. de Baere, B.P. Leroy, W. Bergen, K. Rohrschneider and C.B. Hoyng for sharing patient samples; and the Marshfield Mammalian Genotyping Service for carrying out genotyping in the Pakistani families. This research was supported by grants from The Netherlands Organisation for Scientific Research (916.56.160 to A.I.d.H.); the Foundation Fighting Blindness USA (BR-GE-0606-0349-RAD to A.I.d.H.); the Dutch Kidney Foundation (C04.2112 to R.R.); Landelijke Stichting voor Blinden en Slechtzienden (to A.I.d.H. and F.P.M.C.); Algemene Nederlandse Vereniging ter Voorkoming van Blindheid (to A.I.d.H., R.R. and F.P.M.C); Rotterdamse Vereniging Blindenbelangen (to R.R. and F.P.M.C.); Stichting Blindenhulp (to R.R. and F.P.M.C.); Stichting OOG (to R.R. and F.P.M.C.); the British Retinitis Pigmentosa Society (GR552 to R.R.); the European Union 6th Framework RETNET (MRTNCT-2003-504003 to F.P.M.C. and M.U.), EVI-GENORET (LSHG-CT-2005 512036 to M.U., F.P.M.C. and R.R.) and INTERACTION PROTEOME (LSHG-CT-2003-505520 to M.U.); the Wellcome Trust (061682 and 073477 to C.F.I. and M.D.M., and 068579 to M.E.C.); Yorkshire Eye Research (006 to C.F.I.); the Foundation Fighting Blindness Canada (to R.K.K. and F.P.M.C.); the Fonds de la Recherche en Santé Québec; TD Financial Group (to R.K.K.); Foundation of Retinal Research; The Grousbeck Foundation; The Edel and Krieble Funds; the Ort Family Foundation (to I.H.M., S.D. and R.K.K.); Pro Retina Germany (to M.U. and R.R.); Deutsche Forschungsgemeinschaft (Wo 548-6 to U.W.), FAUN-Stiftung (to U.W.) and Forschung contra Blindheit (to U.W.).

COMPETING INTERESTS STATEMENT

The authors declare no competing financial interests.

Published online at http://www.nature.com/naturegenetics
Reprints and permissions information is available online at http://npg.nature.com/reprintsandpermissions

1. Dharmaraj, S. *et al.* A novel locus for Leber congenital amaurosis maps to chromosome 6q. *Am. J. Hum. Genet.* **66**, 319–326 (2000).
2. Mohamed, M.D. *et al.* Progression of phenotype in Leber's congenital amaurosis with a mutation at the LCA5 locus. *Br. J. Ophthalmol.* **87**, 473–475 (2003).
3. Ostrowski, L.E. *et al.* A proteomic analysis of human cilia: identification of novel components. *Mol. Cell. Proteomics* **1**, 451–465 (2002).
4. Gherman, A., Davis, E.E. & Katsanis, N. The ciliary proteome database: an integrated community resource for the genetic and functional dissection of cilia. *Nat. Genet.* **38**, 961–962 (2006).
5. Giessl, A. *et al.* Differential expression and interaction with the visual G-protein transducin of centrin isoforms in mammalian photoreceptor cells. *J. Biol. Chem.* **279**, 51472–51481 (2004).
6. Guarguaglini, G. *et al.* The forkhead-associated domain protein Cep170 interacts with Polo-like kinase 1 and serves as a marker for mature centrioles. *Mol. Biol. Cell* **16**, 1095–1107 (2005).
7. Quintyne, N.J. *et al.* Dynactin is required for microtubule anchoring at centrosomes. *J. Cell Biol.* **147**, 321–334 (1999).
8. Burakov, A., Nadezhdina, E., Slepchenko, B. & Rodionov, V. Centrosome positioning in interphase cells. *J. Cell Biol.* **162**, 963–969 (2003).
9. Rigaut, G. *et al.* A generic protein purification method for protein complex characterization and proteome exploration. *Nat. Biotechnol.* **17**, 1030–1032 (1999).
10. Shinmura, K., Tarapore, P., Tokuyama, Y., George, K.R. & Fukasawa, K. Characterization of centrosomal association of nucleophosmin/B23 linked to Crm1 activity. *FEBS Lett.* **579**, 6621–6634 (2005).
11. Ma, Z. *et al.* Interaction between ROCK II and nucleophosmin/B23 in the regulation of centrosome duplication. *Mol. Cell. Biol.* **26**, 9016–9034 (2006).
12. Zhang, H. *et al.* B23/nucleophosmin serine 4 phosphorylation mediates mitotic functions of polo-like kinase 1. *J. Biol. Chem.* **279**, 35726–35734 (2004).
13. Shu, X. *et al.* RPGR ORF15 isoform co-localizes with RPGRIP1 at centrioles and basal bodies and interacts with nucleophosmin. *Hum. Mol. Genet.* **14**, 1183–1197 (2005).
14. Ginisty, H., Sicard, H., Roger, B. & Bouvet, P. Structure and functions of nucleolin. *J. Cell Sci.* **112**, 761–772 (1999).
15. Li, D., Dobrowolska, G. & Krebs, E.G. The physical association of casein kinase 2 with nucleolin. *J. Biol. Chem.* **271**, 15662–15668 (1996).
16. Hollander, B.A., Liang, M.Y. & Besharse, J.C. Linkage of a nucleolin-related protein and casein kinase II with the detergent-stable photoreceptor cytoskeleton. *Cell Motil. Cytoskeleton* **43**, 114–127 (1999).
17. Lim, A.C., Tiu, S.Y., Li, Q. & Qi, R.Z. Direct regulation of microtubule dynamics by protein kinase CK2. *J. Biol. Chem.* **279**, 4433–4439 (2004).
18. Faust, M., Gunther, J., Morgenstern, E., Montenarh, M. & Gotz, C. Specific localization of the catalytic subunits of protein kinase CK2 at the centrosomes. *Cell. Mol. Life Sci.* **59**, 2155–2164 (2002).
19. Schermer, B. *et al.* Phosphorylation by casein kinase 2 induces PACS-1 binding of nephrocystin and targeting to cilia. *EMBO J.* **24**, 4415–4424 (2005).
20. Hu, J., Bae, Y.K., Knobel, K.M. & Barr, M.M. Casein kinase II and calcineurin modulate TRPP function and ciliary localization. *Mol. Biol. Cell* **17**, 2200–2211 (2006).
21. Mhawech, P. 14–3-3 proteins—an update. *Cell Res.* **15**, 228–236 (2005).
22. Pietromonaco, S.F., Seluja, G.A., Aitken, A. & Elias, L. Association of 14–3-3 proteins with centrosomes. *Blood Cells Mol. Dis.* **22**, 225–237 (1996).
23. Chen, C.Y., Olayioye, M.A., Lindeman, G.J. & Tang, T.K. CPAP interacts with 14–3-3 in a cell cycle-dependent manner. *Biochem. Biophys. Res. Commun.* **342**, 1203–1210 (2006).
24. Chang, B. *et al.* In-frame deletion in a novel centrosomal/ciliary protein CEP290/NPHP6 perturbs its interaction with RPGR and results in early-onset retinal degeneration in the *rd16* mouse. *Hum. Mol. Genet.* **15**, 1847–1857 (2006).
25. den Hollander, A.I. *et al.* Mutations in the *CEP290* (*NPHP6*) gene are a frequent cause of Leber congenital amaurosis. *Am. J. Hum. Genet.* **79**, 556–561 (2006).
26. Sayer, J.A. *et al.* The centrosomal protein nephrocystin-6 is mutated in Joubert syndrome and activates transcription factor ATF4. *Nat. Genet.* **38**, 674–681 (2006).
27. Valente, E.M. *et al.* Mutations in *CEP290*, which encodes a centrosomal protein, cause pleiotropic forms of Joubert syndrome. *Nat. Genet.* **38**, 623–625 (2006).
28. van Wijk, E. *et al.* The *DFNB31* gene product whirlin connects to the Usher protein network in the cochlea and retina by direct association with USH2A and VLGR1. *Hum. Mol. Genet.* **15**, 751–765 (2006).
29. Roepman, R. *et al.* Interaction of nephrocystin-4 and RPGRIP1 is disrupted by nephronophthisis or Leber congenital amaurosis-associated mutations. *Proc. Natl. Acad. Sci. USA* **102**, 18520–18525 (2005).
30. Brandstatter, J.H., Koulen, P., Kuhn, R., van der, P.H. & Wassle, H. Compartmental localization of a metabotropic glutamate receptor (mGluR7): two different active sites at a retinal synapse. *J. Neurosci.* **16**, 4749–4756 (1996).